UCLA
COMPUTATIONAL AND APPLIED MATHEMATICS

High Frequency Wave Propagation by the Segment Projection Method

Bjorn Engquist
Olof Runborg
Anna-Karin Tornberg

April 2001

CAM Report 01-13

Department of Mathematics
University of California, Los Angeles
Los Angeles, CA. 90095-1555

http://www.math.ucla.edu/applied/cam/index.html

HIGH FREQUENCY WAVE PROPAGATION BY THE SEGMENT PROJECTION METHOD

Björn Engquist*† Olof Runborg‡ Anna-Karin Tornberg*

Abstract

Geometrical optics is a standard technique for the approximation of high frequency wave propagation. Computational methods based on partial differential equations have recently been applied to geometrical optics instead of the traditional ray tracing. These new methods have a number of advantages but typically exhibit difficulties with linear superposition of waves. In this paper we introduce a new partial differential technique based on the segment projection method in phase space. The superposition problem is perfectly resolved and so is the approximation of amplitudes in the neighborhood of caustics. The computational complexity is of the same order as that of ray tracing. The new algorithm is described and a number of computational examples are given including a simulation of wave guides.

Key Words: wave equation, eikonal equation, geometrical optics, segment projection method

Classification: 65M06, 78A05

1 Introduction

High frequency wave propagation is well approximated by asymptotic formulations like geometrical optics and the geometrical theory of diffraction. These formulations can be the basis of computations or they can be used analytically for the understanding of high frequency phenomena.

Let us consider the scalar wave equation,

$$\begin{aligned} \frac{\partial^2 u(\mathbf{x},t)}{\partial t^2} &= c(\mathbf{x})^2 \Delta u(\mathbf{x},t), \quad \mathbf{x} \in \mathbb{R}^d,\ t > 0, \\ u(\mathbf{x},0) &= u_0(\mathbf{x}), \qquad \mathbf{x} \in \mathbb{R}^d, \\ \frac{\partial u(\mathbf{x},0)}{\partial t} &= u_1(\mathbf{x}), \qquad \mathbf{x} \in \mathbb{R}^d. \end{aligned} \tag{1}$$

*Royal Institute of Technology, Department of Numerical Analysis and Computer Science, 10044 Stockholm, Sweden

†University of California, Los Angeles, Department of Mathematics, Los Angeles, California 90095-1555

‡Princeton University, PACM, Department of Mathematics, Princeton, NJ 08544-1000

When u_0 or u_1 contain high frequency components it is customary to use the ansatz,

$$u(\mathbf{x},t) \sim e^{i\omega\varphi(\mathbf{x},t)} \sum_{j=0}^{\infty} a_j(\mathbf{x},t)(i\omega)^j, \tag{2}$$

or,

$$u(\mathbf{x},t) \sim e^{i\omega(\varphi(\mathbf{x})-t)} \sum_{j=0}^{\infty} a_j(\mathbf{x},t)(i\omega)^j, \tag{3}$$

to derive the eikonal equations for the phase φ, [8]. With $\omega \to \infty$ we get from (2),

$$\frac{\partial \varphi}{\partial t} + c(\mathbf{x})|\nabla\varphi| = 0, \tag{4}$$

and from (3),

$$|\nabla\varphi| = \frac{1}{c(\mathbf{x})}. \tag{5}$$

The transport equation for the leading amplitude functions a_0 are for (2) and (3) respectively given by,

$$\frac{\partial a_0}{\partial t} + c\frac{\nabla\varphi\cdot\nabla a_0}{|\nabla\varphi|} + \frac{c^2\Delta\varphi - \frac{\partial^2\varphi}{\partial t^2}}{2c|\nabla\varphi|}a_0 = 0, \tag{6}$$

$$2\nabla\varphi\cdot\nabla a_0 + \Delta\varphi a_0 = 0. \tag{7}$$

Ray tracing can be regarded as the method of characteristics applied to the eikonal equations. The ray $\mathbf{x}(t)$ is parameterized by t and the local direction of the ray is $\mathbf{p} = \nabla\varphi(\mathbf{x}), |\mathbf{p}| = c^{-1} = \eta$,

$$\frac{d\mathbf{x}}{dt} = c^2\,\mathbf{p}, \tag{8}$$

$$\frac{d\mathbf{p}}{dt} = c\nabla_x\eta. \tag{9}$$

The system (8)–(9) can be augmented by an equation for the amplitude and approximated by standard numerical methods for ordinary differential equations.

Ray tracing techniques have difficulties with resolution in regions of diverging rays so simulations based directly on the eikonal equation have recently been introduced, [19, 20, 7].

The eikonal equation is of Hamilton-Jacobi type and has a unique viscosity solution, [4]. This means that the phase has a unique value and that crossing

rays or linear superposition of waves are not allowed. The viscosity solution only gives the first arriving ray or wave front.

One way to resolve this problem is to geometrically decompose the region of the independent variables where there should be multiple rays. Extra eikonal equation computations can be performed in these domains to approximate each separate wave field in the superposition. This was briefly discussed in [5] and more systematically developed by Benamou [1, 2] and Symes [16].

It is possible to derive a Vlasov type partial differential equation from (8), (9), which gives the amplitude and allows for superposition, [10],

$$\frac{\partial w}{\partial t} + c^2 \mathbf{p} \cdot \nabla_x w + c \nabla_x \eta \cdot \nabla_p w = 0. \tag{10}$$

The density $w = w(\mathbf{x}, \mathbf{p}, t)$ is a function of location, the ray vector and time. It is related to the amplitude as $a_0^2 = \int w d\mathbf{p}$. If w has support on $|\mathbf{p}| = c^{-1}$ initially this will be valid for all time and w can be regarded as a function of $\mathbf{p}/|\mathbf{p}|$ and thus of 6 independent variables for $\mathbf{x} \in \mathbb{R}^3$.

When (10) is used for simulations the drawback is the computational complexity. Let h be of the order of the numerical step size for the independent variables. The computational complexity is $O(h^{-6})$ in $\mathbb{R}^3$ and $O(h^{-4})$ in $\mathbb{R}^2$ for an explicit difference method approximating (10). This should be compared to simulations based on ray tracing for the time harmonic problem. The corresponding complexities for the same resolutions are $O(h^{-3})$ in $\mathbb{R}^3$ and $O(h^{-2})$ in $\mathbb{R}^2$. The complexities for explicit approximations of the eikonal equation (4) is $O(h^{-4})$ in $\mathbb{R}^3$ and $O(h^{-3})$ in $\mathbb{R}^2$. The fast marching method, [13], can be used for (1.4) and the complexity is reduced to $O(h^{-3} \log h)$ and $O(h^{-2} \log h)$ respectively.

A different approach was taken in [6, 11]. The eikonal equation is replaced by a system of nonlinear conservation laws that allows for a limited number of linear superpositions. The conservation laws are derived by integrating equation (10) with respect to $\mathbf{p}$ and using the finite number of superpositions as closure. The number of independent variables is then reduced to four in $\mathbb{R}^3$ and three in $\mathbb{R}^2$ but the numerical approximations exhibit problems when there are several crossing rays. See also [3] for the technique of reducing the number of independent variables.

Another method was introduced by Steinhoff and collaborators in [14, 15] and further refined by Ruuth et al. in [12]. The dependent variables in this technique are essentially the coordinates of the closest point on a wave front from a given $\mathbf{x}$-coordinate. This clever choice of representation and a time stepping scheme following the rules of geometrical optics allows for linear superposition. The present forms of the method have higher complexity than ray tracing and certain cases will not be correctly described. One such example is a wave front given by a collapsing circle with two parallel tangent lines. When the circle and the tangent lines have been reduced to one line the information of the circle is lost and cannot be recovered. The method is quite straight forward and is being further developed.

The new technique we introduce here is also based on the tracking of fronts, but it is done in phase space. In two space dimensions a front is given as a curve in $xy\theta$-space where $\theta = \cos^{-1}(p_1/|\mathbf{p}|)$ is the angle between the normal of the front and the x-axis. The curve is represented by its projection onto the two dimensional $xy, x\theta$ and $y\theta$ spaces. The representation of the curve in each of these spaces is evolved by the segment projection method [17]. The segment projection method determines the motion of the curve by the solution of partial differential equations in one space variable.

The segment projection method allows for the superposition of fronts and the use of the phase plane makes it possible to describe caustics, including a correctly approximated amplitude. In spite of the extension to the phase plane the computational complexity is not more than that of standard ray tracing. This is a result of the projection onto the lower dimensional spaces. In the segment projection a curve in two dimensions is represented as a union of segments. These segments are chosen such that they can be given as a function of one of the variables.

The general form of the segment projection method for one dimensional curves in $\mathbb{R}^2$ and $\mathbb{R}^3$ is given in section two. This is followed, in section three, by a presentation of the method adapted to geometrical optics. The final section contains numerical examples. In these sections we shall use the notation $\mathbf{x} = (x_1, x_2)$ or $\mathbf{x} = (x, y)$ whenever convenient.

2 The Segment Projection Method

The segment projection method is a computational method for tracking the dynamic evolution of interfaces. It was recently developed in [17, 18]. The basic idea is to represent a curve or surface as a union of segments. Each segment is chosen such that it can be given as a function of the independent variables. The representation is thus analogous to a manifold being defined by an atlas of charts. The motions of the individual segments are given by partial differential equations based on the physics describing the evolution of the interfaces.

General software has been developed for curves γ in $\mathbb{R}^2$ and we shall give a brief overview of the method. The segments are here represented by functions $Y_j(x)$ and $X_k(y)$. The domains of the independent variables of these functions are projections of the segments onto the coordinate axis. The coordinates of the points on γ are given by $(x, y) = (x, Y_j(x))$ or $(x, y) = (X_k(y), y)$. For each point on a curve γ, there is a least one segment defining the curve. To make the description complete, information about the connectivity of segments must also be provided.

The number of segments needed to describe a curve depends on the shape of the curve. An extremum of a function $Y_j(x)$ defines a separation point for the y-segments, as no segment given as a function of y can continue past this point. Similarly, an extremum of a function $X_k(y)$ defines a separation point for the x-segments. A sketch of a distribution of segments is shown in figure 1. For moving interfaces $Y_j = Y_j(x, t)$ and $X_k = X_k(y, t)$ are also functions of time.

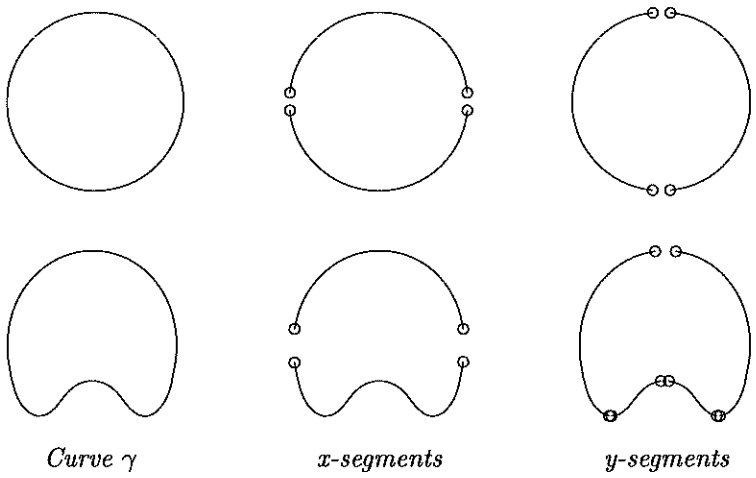

Figure 1: Segment structure for circle and deformed circle.

The segments are moved by equations of motion, and after each numerical advection step, the segment representation is reinitialized. Dynamic creation and elimination of segments are employed to follow the evolution of the curves. New segments are created if new extrema have appeared, and segments are removed when extrema disappear. The connectivity of segments must be kept updated. If we assume that the lower deformed circle in figure 1 has evolved from the circle above, a new maximum and a two new minima have appeared in the lower x-segment. The number of y-segments should then be increased as is seen in the figure.

For each segment, the domain of the independent variable must be defined. These segments are numerically given by arrays for Y_j and X_k. The domains of the independent variables, the arrays and information about connectivity between the segments, define the structure that represents the curve.

From the definition of an x-segment, an ordered set of numbers is created that contains the start and end points of the segment, together with the extremum points of the segment. The intervals between these points correspond to different segments of the other variable. It is necessary to keep track of the connections between these segments.

Very short segments are not practical to work with for the evolution of γ. They are, however, needed in the structure of connectivity and are defined as empty segments. If the difference between two consecutive extrema in Y_j is less than $2\,\Delta y$ in absolute value, the corresponding y-segment is defined as empty.

Let a velocity field $\mathbf{u} = (u, v)^T$ be given by which the curve should move. The segments $y = Y(x, t)$ and $x = X(y, t)$ are updated according to the partial

differential equations,

$$\frac{\partial Y}{\partial t} + u\frac{\partial Y}{\partial x} = v, \tag{11}$$

$$\frac{\partial X}{\partial t} + v\frac{\partial X}{\partial y} = u. \tag{12}$$

Note that there is only one spatial variable present in both these equations. Quantities that are transported by the velocity field can also be defined as functions on the segments. Let $\mathcal{F}^t(x,y)$ be the flow generated by $\mathbf{u}$. If $r(t,x,y)$ evolves according to the ODE $dr(t,\mathcal{F}^t)/dt = h(t,\mathcal{F}^t,r(t,\mathcal{F}^t))$, for fixed (x,y), then

$$\frac{\partial R^x}{\partial t} + u\frac{\partial R^x}{\partial x} = h(t,x,Y,R^x), \tag{13}$$

$$\frac{\partial R^y}{\partial t} + v\frac{\partial R^y}{\partial y} = h(t,X,y,R^y), \tag{14}$$

where $R^x(t,x) = r(t,x,Y(t,x))$ and $R^y(t,y) = r(t,Y(t,y),y)$.

Boundary conditions must be defined for the segments. They are either given in the original problem formulation or interpolated from an overlapping segment in the other coordinate direction.

After the numerical advection step based on (11,12), we need to review the segment structure. If no new extrema have appeared, and no old have disappeared, no change needs to be made in the structure of the segments. We need, however, to update the positions of the extremum points, and correct the corresponding segment information according to this. If new extrema have appeared or disappeared, the structure of the segments defined as functions of the other spatial variable needs to be modified.

Any moving curve γ is represented by overlapping segments. These segments evolve individually and may separate slightly in the overlapping regions due to numerical errors. A reinitialization is applied in every time step to realign the segments. This is done by a weighted interpolation. A segment will typically yield the most accurate description of the curve if its slope is small.

For a given point x_k, an x-segment has the value $f_k = Y(x_k,t)$. Denote by $\tilde{f}_k$, the value at x_k, interpolated from the discretized segment in the y-direction. Compute the slope of the two segments at this point and denote the average by s_k. The new value at x_k is set to

$$f_k^{\text{new}} = f_k + \theta(s_k)(\tilde{f}_k - f_k), \tag{15}$$

where the weight $\theta(s)$ is a function of the slope s, given by:

$$\theta(s) = \begin{cases} 0 & \text{for } s < 1/\beta, \\ \frac{\beta}{\beta^2-1}(s - 1/\beta) & \text{for } 1/\beta \le s \le \beta, \\ 1 & \text{for } s > \beta. \end{cases} \tag{16}$$

The default value of β is 2. The same interpolation is also applied to the functions R^x and R^y that are defined on the segments.

When different parts of γ cross each other, geometric rules for the segment interaction must be given. Examples are the merging of two bubbles in multi-phase flow and the reflection of a wave front γ_1 meeting a curve γ_2, representing a perfect reflector.

The advection and reinitialization process for a structure of segments, representing a curve γ, can be summarized as follows:

(1) Advect all x- and y-segments from a velocity field $\mathbf{u} = (u, v)$ and evolve associated quantities defined on the segments by numerical approximations of (11)–(14).

(2) Update the segment structure. For each segment:

- Check if any new extrema have appeared, or if any extrema have disappeared. Split or merge corresponding segments of the other coordinate.
- Review the use of empty segments. Add or remove short segments, as described above.
- Use the position of the extrema to update the start index and the stop index of the independent variable for the segment of the other coordinate.

(3) For each segment whose domain of definition have increased, new values need to be defined. These are interpolated from the corresponding segment in the opposite direction.

(4) Interpolate segment between overlapping parts of the x and y segments. The new values are assigned using a weight function based on the slopes of the segments.

(5) Rearrange the segment structure from the rules of segment interactions.

These steps are generic and essentially the same for different applications. A common software will thus apply to different problems with only minor modifications, for example, in the advection and the interaction algorithms.

Curves of co-dimension two in $\mathbb{R}^3$ are approximated by their projections onto the two dimensional coordinate planes. If a curve,

$$\gamma(t) : \{X_1(s,t), X_2(s,t), X_3(s,t)\},$$

is parameterized by s and evolves by the velocity field

$$\mathbf{u}(\mathbf{x}, t) = (u_1(\mathbf{x}, t), u_2(\mathbf{x}, t), u_3(\mathbf{x}, t)),$$

we have,

$$\frac{dX_j}{dt} = u_j(\mathbf{X}, t), \quad j = 1, 2, 3.$$

Let the projection of γ onto the $x_j x_k$-plane be represented by a set of segment functions of the type $x_j = X^{jk}(x_k, t)$ and $x_k = X^{kj}(x_j, t)$. The evolution of the segment functions in all three projection planes is then given by the equations,

$$\frac{\partial X^{jk}}{\partial t} + u_k \frac{\partial X^{jk}}{\partial x_k} = u_j, \quad j = 1,2,3; \; k = 1,2,3; \; j \neq k. \tag{17}$$

The projections in the $x_j x_k$-planes are updated in time following the steps (1)-(5) above. A sixth step is then added with interpolation between the representations in the three coordinate planes. This step is similar to step (4) and could be needed in order to define u_k and u_j in (17). The simulations presented in this paper do not require such interpolations.

There is yet no general software for two dimensional surfaces in $\mathbb{R}^3$. The principle is analogous to the lower dimensional case. The surface Σ is represented by functions defined on the three coordinate planes. The functions $x_\ell = X_\ell^{jk}(x_j, x_k, t)$ define the segments as in $\mathbb{R}^2$ and the union of segments defines Σ. Given the velocity field $\mathbf{u}(\mathbf{x}, t)$, the motion of the segments is given by,

$$\frac{\partial X_\ell^{jk}}{\partial t} + u_j \frac{\partial X_\ell^{jk}}{\partial x_j} + u_k \frac{\partial X_\ell^{jk}}{\partial x_k} = u_\ell,$$
$$j = 1,2,3, \; k = 1,2,3, \; \ell = 1,2,3, \; j \neq k, j \neq \ell, k \neq \ell.$$

3 The Segment Projection Method for Geometrical Optics

The segment projection method will be applied to track the evolution in phase space of fronts that are given by geometrical optics. For two space dimensions a curve γ in $\mathbb{R}^3$ is tracked and for three space dimensions a surface Σ in $\mathbb{R}^5$ is evolved. We shall mainly discuss the two-dimensional case and only give one three-dimensional example in section 4.2. Section 3.1 discusses how to reduce the two-dimensional case to just one dimension. In the presentation of the method, we may assume that γ or Σ and their projections are functions. The segment projection technique will reduce the general case to a set of segments that are functions of some of the independent variables.

Let the independent variables be x, y and θ. The orthogonal projections of γ onto the xy, $x\theta$ and $y\theta$-planes are denoted by $\gamma_{xy}, \gamma_{x\theta}$ and $\gamma_{y\theta}$ respectively. The evolution of $\gamma = \gamma(t)$ will be determined by the two-dimensional segment projection method as presented in section 2.

In figure 2, left frame, an initial circular wave front is given in the xy-plane. this frame also displays the phase plane curve γ in $\mathbb{R}^3$ together with its $x\theta$-and $y\theta$-projections. Let the circular wave front contract with time and be focused to a point $(x, y) = (1, 1)$ at time $t = 1$, $c(\mathbf{x}) \equiv 1$. The representations of γ at $t = 1$ in the $x\theta$-and $y\theta$-planes are smooth and the evolution can easily be continued to $t > 1$.

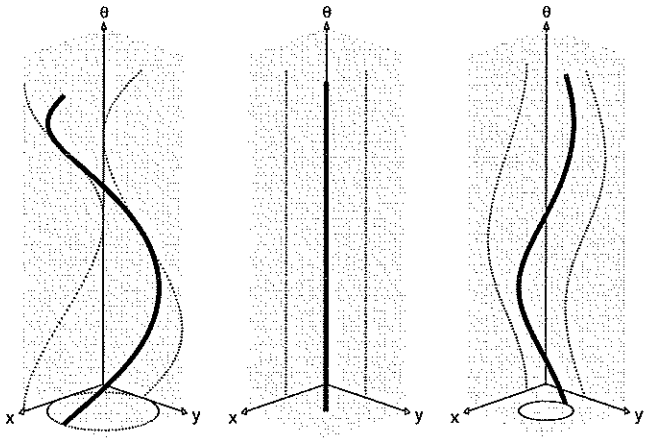

Figure 2: Phase plane curve γ: thick line, with projections onto xy-, $x\theta$- and $y\theta$-planes; left frame: initial circular wave front, $t = 0$; middle frame: focus at $t = 1$; right frame: $t = 1.5$.

The evolution of a wave front in the xy-plane is given by the velocity $c(\mathbf{x})$ in its normal direction $\mathbf{n}$. The velocity field $\mathbf{u} = (u, v)$ in the xy-plane is thus

$$(u, v) = c(\mathbf{x})\mathbf{n} = c(\mathbf{x})\,(\cos\theta, \sin\theta), \tag{18}$$

where θ is the angle between the normal vector and the x-axis. The normal vector can be computed from the segment functions.

From the general equations (11)–(12) and the velocity field (18), we get the Eulerian form of the evolution equations for the x- and y-segments in the xy-plane respectively,

$$\begin{cases} \dfrac{\partial Y^x}{\partial t} + c(x, Y^x(x,t))\,\cos\theta\,\dfrac{\partial Y^x}{\partial x} = c(x, Y^x(x,t))\sin\theta, \\ \dfrac{\partial X^y}{\partial t} + c(X^y(y,t), y)\,\sin\theta\,\dfrac{\partial X^y}{\partial y} = c(X^y(y,t), y)\cos\theta, \end{cases} \tag{19}$$

The approach of tracking the front only in the xy-plane, computing θ from the segments, breaks down at caustics. Therefore, the front must be tracked in phase space, and the other two projections are needed.

With $\mathbf{p} = (\cos\theta, \sin\theta)/c(\mathbf{x})$ we can derive from (8, 9),

$$\frac{d\theta}{dt} = \frac{\partial c}{\partial x}\sin\theta - \frac{\partial c}{\partial y}\cos\theta. \tag{20}$$

This equation, together with (18) give the velocity field needed to apply (11)–(12) for the segment equations in the $x\theta$ and $y\theta$-planes.

Let the x and θ segments in the $x\theta$-plane be denoted by Θ^x and X^θ and the y and θ segments in the $y\theta$-plane be Θ^y and Y^θ respectively. The segment equations are,

$$\begin{cases} \dfrac{\partial \Theta^x}{\partial t} + c\cos\theta \dfrac{\partial \Theta^x}{\partial x} = \alpha, \\ \dfrac{\partial X^\theta}{\partial t} + \alpha \dfrac{\partial X^\theta}{\partial \theta} = c\cos\theta, \end{cases} \tag{21}$$

$$\begin{cases} \dfrac{\partial \Theta^y}{\partial t} + c\sin\theta \dfrac{\partial \Theta^y}{\partial y} = \alpha, \\ \dfrac{\partial Y^\theta}{\partial t} + \alpha \dfrac{\partial Y^\theta}{\partial \theta} = c\sin\theta, \end{cases} \tag{22}$$

$$\alpha = \frac{\partial c(\mathbf{x})}{\partial x}\sin\theta - \frac{\partial c(\mathbf{x})}{\partial y}\cos\theta. \tag{23}$$

The one dimensional hyperbolic equations above, are easily solved by standard numerical methods. Note that the representation of the phase plane curve γ may be degenerate for the projection onto one of the coordinate planes, but there will always be two projections for which γ is well represented.

When η is constant the amplitude on the curve can easily be calculated by post-processing of the results from (21,22). By (10), the intensity, $A^2 = \int w d\mathbf{p}$, is a conserved quantity in time, and changes (pointwise) only through geometrical spreading. Consider for instance an initial curve $(x(\theta), y(\theta), \theta)$ with amplitude $A_0(\theta)$, moving in the normal direction $(\cos\theta, \sin\theta)^T$. At time t it will have evolved to $(x(\theta) + t\cos\theta, y(\theta) + t\sin\theta, \theta)$. Let $J(\theta, t)$ be the Jacobian of the mapping $(x, y) \mapsto (x + t\cos\theta, y + t\sin\theta)$ and set $q = |\det J|$. Then the amplitude at time t is given by

$$A^2(\theta, t) = \frac{A_0^2(\theta) q(\theta, 0)}{q(\theta, t)},$$

and since $(x_\theta, y_\theta) \perp (\cos\theta, \sin\theta)$ by construction,

$$q(\theta, t) = |x_\theta y_t - y_\theta x_t| = |x_\theta \sin\theta - y_\theta \cos\theta| = \left((x_\theta(\theta, t))^2 + (y_\theta(\theta, t))^2\right)^{1/2}.$$

We note finally that q can be computed from $X^\theta(\theta, t)$ and $Y^\theta(\theta, t)$ in (21,22).

3.1 Reduction to One Dimension

In many problems the x-component of the ray vector is always positive and the x-axis can thus be used as evolution direction. Time is not explicitly needed in the calculation and θ can be computed as a function of x and y, and y as a function of x and θ. From (8,9,20) we get the velocity field for this setting,

$$\mathbf{u} = (u, v)^T = \left(\tan\theta, \ \frac{1}{\eta}(\eta_y - \eta_x \tan\theta)\right)^T,$$

and the partial differential equation for the segments $\theta = \Theta(x,y)$ and $y = Y(x,\theta)$ are

$$\frac{\partial \Theta}{\partial x} + u\frac{\partial \Theta}{\partial y} = v,$$
$$\frac{\partial Y}{\partial x} + v\frac{\partial Y}{\partial \theta} = u.$$

The arrival time, T, is now a quantity defined on the phase plane curve, and it can be computed according to (13,14). Let $\mathcal{F}^x(y,\theta) = (\mathcal{F}_1^x, \mathcal{F}_2^x)^T$ be the flow generated by $\mathbf{u}$. By inverting (8), we see that $dT(x,\mathcal{F}^x)/dx = \eta/\cos\theta$. This yields the following differential equations, defined for the y-segments and θ-segments respectively,

$$\frac{\partial T^y}{\partial x} + u\frac{\partial T^y}{\partial y} = \frac{\eta}{\cos\theta},$$
$$\frac{\partial T^\theta}{\partial x} + v\frac{\partial T^\theta}{\partial \theta} = \frac{\eta}{\cos\theta}.$$

To derive the equations for the amplitude, we consider the reduced form of (10) for the phase space density $w = w(x,y,\theta)$,

$$\frac{\partial w}{\partial x} + u\frac{\partial w}{\partial y} + v\frac{\partial w}{\partial \theta} = 0, \tag{24}$$

where again, the amplitude is given by $A^2 = \int w d\theta$. Suppose the initial wave at $x = 0$ is a curve in the phase plane defined by $G(y,\theta) = 0$ with amplitude $A_0(y,\theta)$. This corresponds to the initial data

$$w(0,y,\theta) = w_0(y,\theta) = A_0^2(y,\theta)\,\delta(G(y,\theta))\,|G_\theta(y,\theta)|$$

for (24) whose solution is then $w(x,y,\theta) = w_0(\mathcal{F}^{-x}(y,\theta))$. When Θ is well defined, $G(\mathcal{F}^{-x}(y,\Theta(x,y))) = 0$, and the amplitude on the segment is given by

$$\begin{aligned} A^2(x,y) &= \int w_0\left(\mathcal{F}^{-x}(y,\theta)\right) d\theta = \frac{A_0^2(\mathcal{F}^{-x})|G_\theta(\mathcal{F}^{-x})|}{\left|\nabla_{y\theta} G(\mathcal{F}^{-x}) \cdot \frac{\partial \mathcal{F}^{-x}}{\partial \theta}\right|}\,(y,\Theta(x,y)) \\ &= \frac{A_0^2(\mathcal{F}^{-x})|G_\theta(\mathcal{F}^{-x})|\,|\det \mathcal{J}^x|}{\left|G_y(\mathcal{F}^{-x})\frac{\partial \mathcal{F}_1^x}{\partial \theta} - G_\theta(\mathcal{F}^{-x})\frac{\partial \mathcal{F}_1^x}{\partial y}\right|}\,(y,\Theta(x,y))\,. \end{aligned}$$

where $\mathcal{J}^x$ is the Jacobian of $\mathcal{F}^x$. The same equality holds when $(y,\Theta(x,y))$ is replaced by $(Y(x,\theta),\theta)$. In order to compute $A(x,y)$ we must hence also evolve $\mathcal{F}^{-x}$ and $\mathcal{J}^x$ as quantities on the curve. Let $D\mathbf{u}$ be the Jacobian of $\mathbf{u}(x,y,\theta)$ with respect to (y,θ). We have,

$$\frac{d\mathcal{F}^{-x}(\mathcal{F}^x)}{dx} = 0, \qquad \frac{d\mathcal{J}^x(\mathcal{F}^x)}{dx} = D\mathbf{u}(\mathcal{F}^x)\mathcal{J}^x(\mathcal{F}^x),$$

The quantities are then given by the PDEs

$$\frac{\partial F^y}{\partial x} + u\frac{\partial F^y}{\partial y} = 0, \qquad \frac{\partial J^y}{\partial x} + u\frac{\partial J^y}{\partial y} = D\mathbf{u}J^y,$$
$$\frac{\partial F^\theta}{\partial x} + v\frac{\partial F^\theta}{\partial \theta} = 0, \qquad \frac{\partial J^\theta}{\partial x} + v\frac{\partial J^\theta}{\partial \theta} = D\mathbf{u}J^\theta.$$

Here, F^y, F^θ give $\mathcal{F}^{-x}$ and J^y, J^θ give $\mathcal{J}^x$ on the segments $\Theta(x,y)$ and $Y(x,\theta)$ respectively. Initial data for those equations are $F^y(0,y) = (y, \Theta(0,y))^T$, $F^\theta(0,\theta) = (Y(0,\theta),\theta)^T$ and $J^y(0,y) = J^\theta(0,\theta) = I$, the identity.

4 Numerical Examples

We shall present four computational examples in order to describe different aspects of the method. All of the examples involve caustics and superposition.

4.1 Contracting Elliptical Wave Front

The initial values in this example correspond to a one dimensional elliptical wave front in $\mathbb{R}^2$, see figure 3. The initial motion is contraction and the index of refraction is constant. The projections of the front in phase space onto the $x\theta$ and $y\theta$-planes are smooth even through caustics, figure 4. The function $\alpha \equiv 0$, (23), which simplifies the calculations. No differential equation needs to be solved in the xy-plane. The equations (21)-(22) are sufficient and the xy-location of the wave front is given by X^θ, Y^θ. There is no problem in calculating the amplitude through the formation of caustics using (3), figure 5.

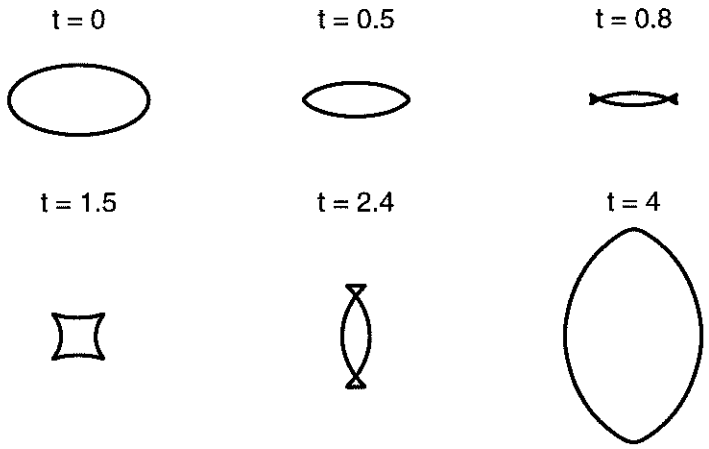

Figure 3: Evolution of an initially elliptical wave front in the xy-plane.

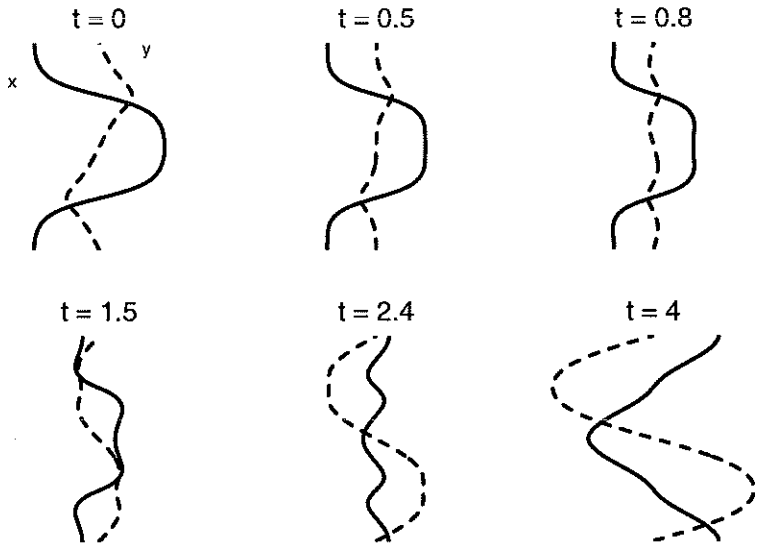

Figure 4: Projection of phase plane curves γ, solid lines: $x\theta$-plane; dashed lines: $y\theta$-plane.

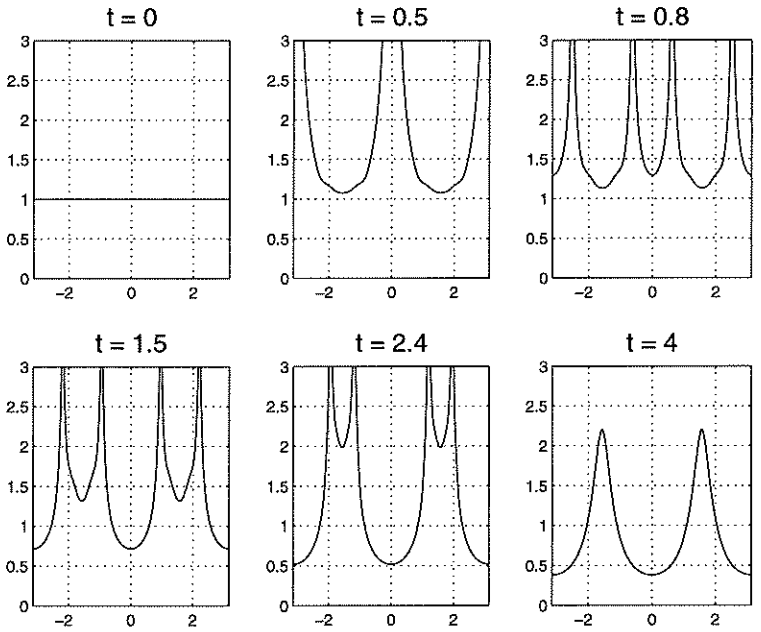

Figure 5: Evolution of amplitude as function of θ.

4.2 Contracting Ellipsoidal Wave Front

The example in section 4.1 is here extended to a surface in $\mathbb{R}^3$. Even though general software for the three dimensional segment projection method has not yet been developed this simulation can be done. In figure 6 we see the evolution of the wave front at different times. The projections of the initial surface in phase space onto the $x\theta_1\theta_2$-, $y\theta_1\theta_2$- and $z\theta_1\theta_2$-spaces are given in figure 7.

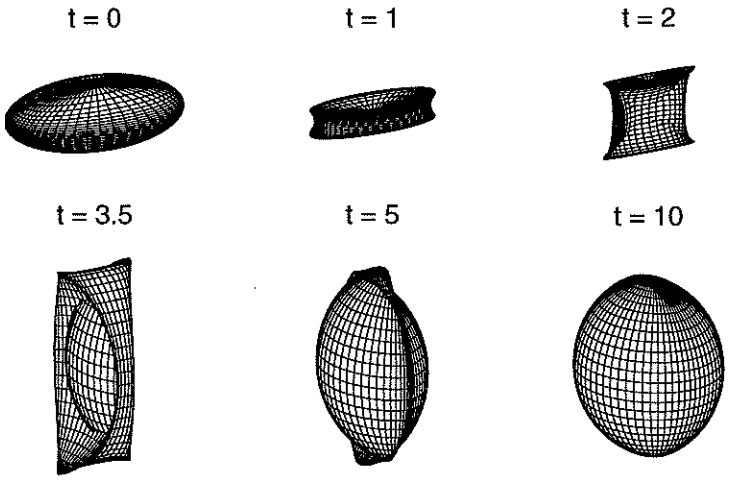

Figure 6: Evolution of wave front in xyz-space.

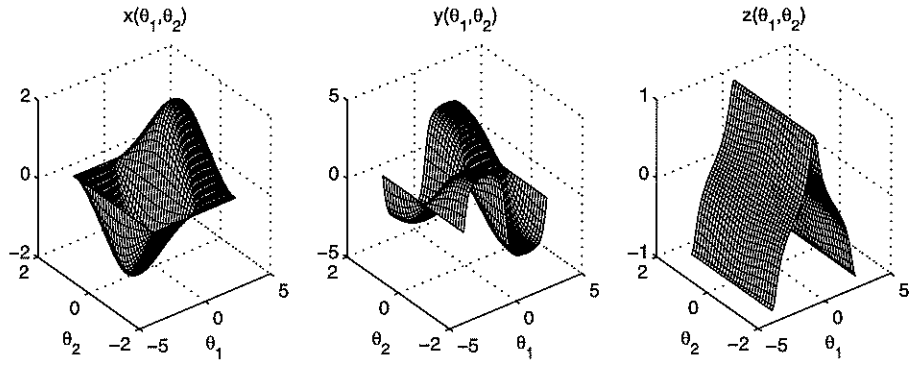

Figure 7: Projections of phase space surface Σ, onto different coordinate planes at t=0.

4.3 Focusing from a Lens

In this example with variable index of refraction a wave front passes through a lens, modeled by the index of refraction

$$\eta(x,y) = 1.5 - \frac{1}{\pi}\arctan\left(5[(y-1)^2 - 0.1(x-0.5)]\right).$$

The left frame in figure 8 shows the direction of the rays and isocurves for the index of refraction. In the right frame, the initial planar wave front is given together with the wave fronts at later times. This includes the development of caustics.

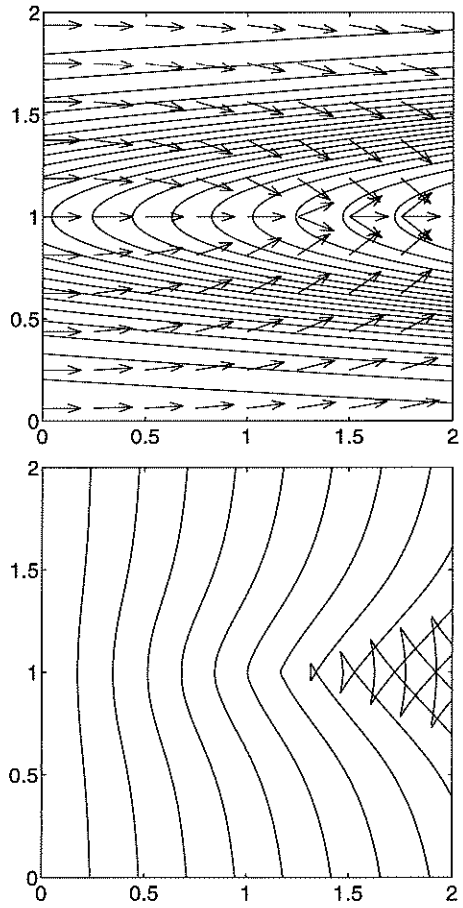

Figure 8: Results for the lens simulation. Left frame: local ray directions with contour lines of index of refraction overlayed; right frame: wave front in the xy-plane for a sequence of arrival times (T-values).

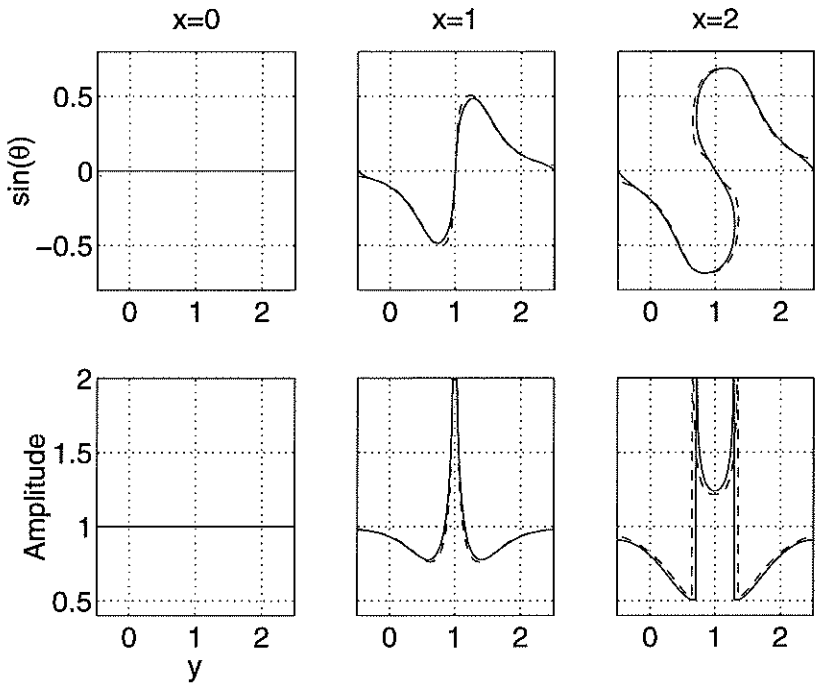

Figure 9: Results at different x-positions for the lens simulation. Upper row: phase plane curve; lower row: amplitude. Solid line: $\Delta y = 0.01$; dashed line: high resolution ray tracing.

Since all rays go in the positive x-direction in this simulation, we can use the reduced model of section 3.1. The calculation of T^y, T^θ is used to determine the wave fronts in figure 8 from interpolation of Θ and Y. Figure 9 compares the results obtained with the segment projection method and a ray traced reference solution in order to give an indication of the numerical error. The segments Θ and Y are given in figure 10.

4.4 Waveguide

In this simulation an incoming plane wave at $x = 0$ with constant amplitude $A = 1$, enters a waveguide. The variable index of refraction in the wave guide, $\eta(x, y) = 1 + \exp(-y^2)$, causes the rays to bend. The ray pattern is given in figure 11. The corresponding local ray directions, amplitude and wave fronts as computed by the segment projection method are in figure 12. The technique described in section 3.1 of having the x-axis as evolution direction is also used in this application. The phase space curve in the $y\theta$-plane becomes complicated at larger x-values but it is still handled well by the segment projection method, see figure 13.

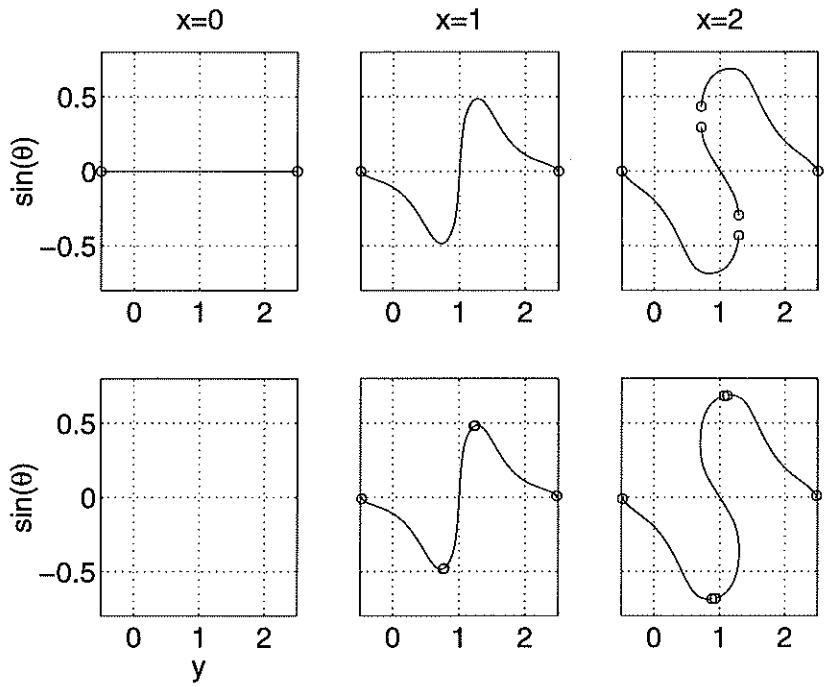

Figure 10: Segment structure for lens simulation corresponding to phase plane curve in figure 9. Upper row: y-segments; lower row: θ-segments.

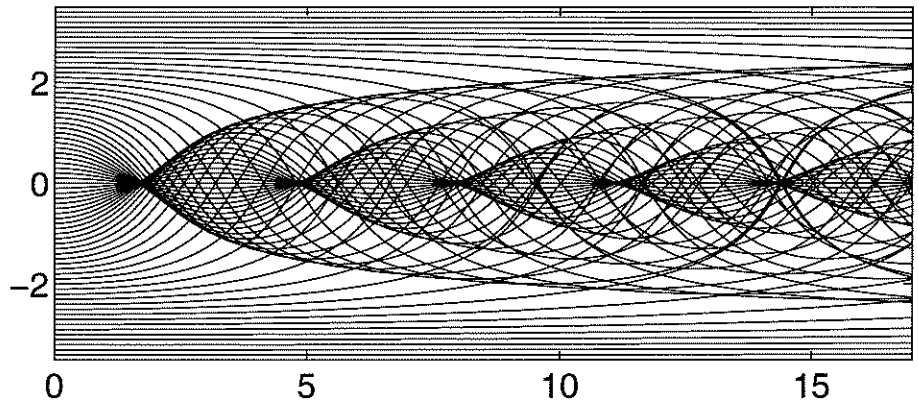

Figure 11: Rays from initial plane wave for wave guide.

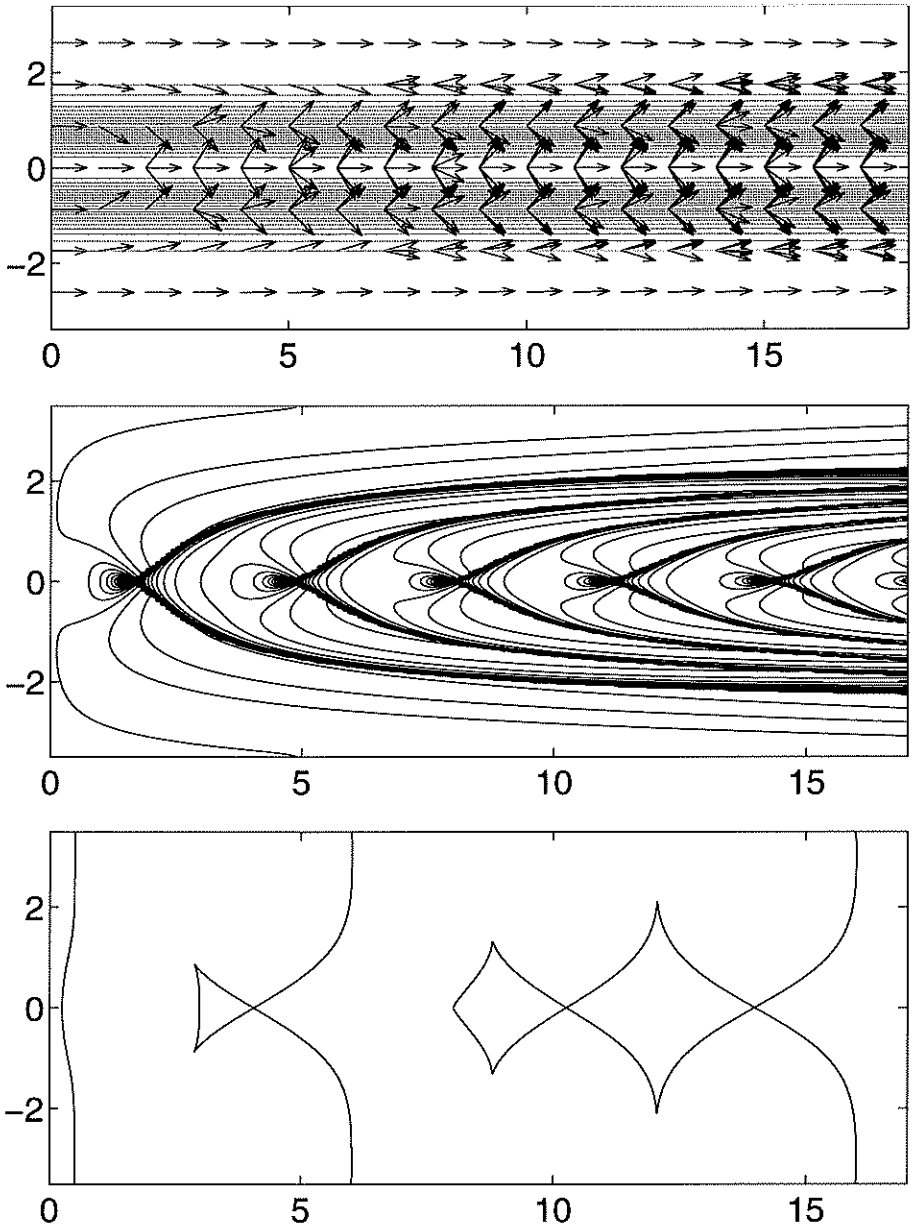

Figure 12: Results for the waveguide simulation. Top frame: local ray directions with contour lines of index of refraction overlayed; middle frame: amplitude, contour lines of $\min(A, 4)$; bottom frame: wave fronts in the xy-plane at $T = 0.5$, 6, 16.

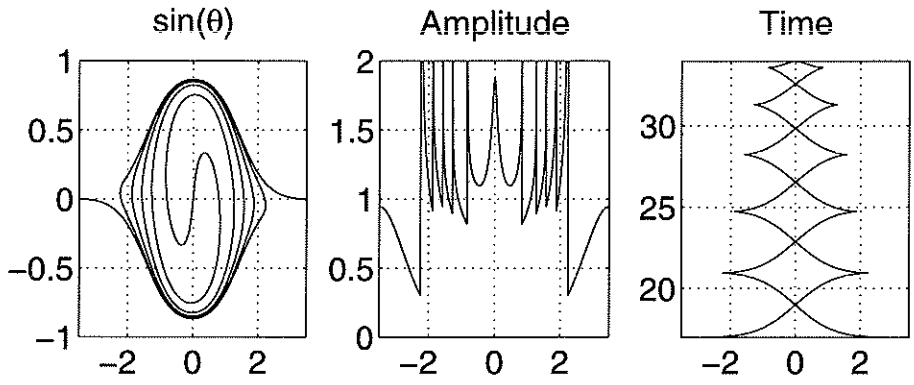

Figure 13: Results for wave guide at $x = 17$ as a function of y; left frame: $\sin(\theta)$; middle frame: amplitude A; right frame: time T.

References

[1] J.-D. Benamou. Big ray tracing: Multivalued travel time field computation using viscosity solutions of the eikonal equation. *J. Comput. Phys.*, 128(4):463-474, 1996.

[2] J.-D. Benamou. Direct solution of multivalued phase space solutions for Hamilton-Jacobi equations. *Comm. Pure Appl. Math.*, 52(11):1443–1475, 1999.

[3] Y. Brenier and L. Corrias. A kinetic formulation for multibranch entropy solutions of scalar conservation laws. *Ann. Inst. H. Poincaré*, 15(2):169-190, 1998.

[4] M. Crandall and P. Lions. Viscosity solution of Hamilton-Jacobi equations. *Trans. Amer. Math. Soc.*, 227:1-42, 1983.

[5] B. Engquist, E. Fatemi and S. Osher. Numerical solution of the high frequency asymptotic expansion for the scalar wave equation. *J. Comput. Phys.*, 120(1):145-155, 1995.

[6] B. Engquist and O. Runborg. Multi-phase computations in geometrical optics. *J. Comput. Appl. Math.*, 74:175-192, 1996.

[7] L. Gosse and F. James. Convergence results for an inhomogeneous system arising in various high frequency approximations. Preprint. 2000.

[8] J. Keller. Geometrical theory of diffraction. *J. Opt. Soc. Am.*, 52, 1962.

[9] S. Osher and J.A. Sethian. Fronts propagating with curvature dependent speed: Algorithms based on Hamilton-Jacobi formulations. *J. Comput. Phys.*, 79:12-29, 1988.

[10] O. Runborg. Multiscale and multiphase methods for wave propagation. Ph.D. Thesis, Department of Numerical Analysis and Computer Science, Royal Institute of Technology (KTH), Stockholm, Sweden, 1998. ISBN 91-7170-318-7, TRITA-NA-9818.

[11] O. Runborg. Some new results in multiphase geometrical optics. *M2AN Math. Model. Numer. Anal.*, 34:1203-1231, 2000.

[12] S.J. Ruuth, B. Merriman and S. Osher. A fixed grid method for capturing motion of self-intersecting wavefronts and related PDEs. *J. Comput. Phys.* 163:1-21, 2000.

[13] J.A. Sethian. Level set methods and fast marching methods: Evolving interfaces in computational geometry, fluid mechanics, computer vision and materials science. Cambridge University Press, 1999.

[14] J. Steinhoff and M. Fan. Eulerian computation of evolving surfaces, curves and discontinuous fields. University of Tennessee Space Institute Report, Tullahoma, TN 37388, 1998.

[15] J. Steinhoff, M. Fan and L. Wang. A new Eulerian method for the computation of propagating short acoustic and electromagnetic pulses. *J. Comput. Phys.*, 157:683-706, 2000.

[16] W. Symes. A slowness matching finite difference method for traveltimes beyond transmission caustics. Preprint, Dept. of Computational and Applied Mathematics, Rice University, 1996.

[17] A.-K. Tornberg. Interface tracking methods with applications to multiphase flows. Ph.D. Thesis, Department of Numerical Analysis and Computer Science, Royal Institute of Technology (KTH), Stockholm, Sweden, 2000. ISBN 91-7170-558-9, TRITA-NA 0010.

[18] A.-K. Tornberg and B. Engquist. Interface tracking in two-phase flows. To appear in *Multifield Problems in Solid and Fluid Mechanics*, Springer Verlag, Berlin.

[19] J. van Trier and W. W. Symes. Upwind finite-difference calculation of traveltimes. *Geophysics*, 56(6):812-821, June 1991.

[20] J. Vidale. Finite-difference calculation of traveltimes. *B. Seismol. Soc. Am.*, 78(6):2062-2076, December 1988.